Supplementary Information

Electro-osmotic vortices promote the capture of folded proteins by PlyAB nanopores

Gang Huang[†], Kherim Willems[‡,§], Mart Bartelds[†], Pol van Dorpe[§,⊥], Misha Soskine[†], Giovanni Maglia*[,†]

[†]Groningen Biomolecular Sciences & Biotechnology Institute, University of Groningen, 9747 AG Groningen, The Netherlands

[‡]KU Leuven Department of Chemistry, Celestijnenlaan 200G, 3001 Leuven, Belgium

[§]imec, Kapeldreef 75, 3001 Leuven, Belgium

[⊥]KU Leuven Department of Physics and Astronomy, Celestijnenlaan 200D, 3001 Leuven, Belgium

Table of Contents

Materials and Methods

Chemicals were purchased from Sigma-Aldrich and Ruth with high purity grade unless otherwise specified. Synthetic genes and primers were ordered from IDT and used without further purification. All enzymes were purchased from Thermo scientific except the RED Polymerase, which was purchased from Sigma-Aldrich. Lipids were obtained from Avanti Polar Lipids. Plasma proteins and bovine serum protein (BSA) were ordered from Sigma-Aldrich.

Pleurotolysin A, B monomer expression and purification

The genes encoding for pleurotolysin A and B (PlyA, PlyB), which also contained six additional histidine residues at the C-terminus, were ligated into a pT7 plasmid between the *NcoI* and *HindIII* restriction sites. The plasmids were then transferred to BL21(DE3) *E.cloni*® competent cell by electroporation. After overnight growth at 37 °C on a LB agar plate containing 100 µg/mL ampicillin, the cells were harvested from the plates and inoculated into 200 mL fresh sterile 2YT media, supplemented with 100 µg/mL ampicillin. The cell culture was grown at 37 °C with 220 rpm shaking until the absorbance of the solution reached 0.56 at 600 nm. Then, 0.5 mM (final) of IPTG was added to the cell culture and the temperature was lowered to 25 °C (220 rpm shaking) for overnight growth. Cells were harvested by centrifugation (2000 × g, 30 minutes) at 4 °C and pellet was stored at -80 °C. Pellet from 100 mL cultures were then resuspended in 30 mL lysis buffer (150 mM NaCl, 15 mM Tris, 1 mM $MgCl_2$, 0.2 mg/ml lysozyme, one cOmplete™ Protease Inhibitor Cocktail tablet and 0.05 units/ml DNase, pH 7.5) and vigorous mixed for 1 hour. Cell lysates were sonicated for 2 minutes (duty cycle 10%, output control 3 using a Branson Sonifier 450) and centrifuged at 4°C (5400 ×g for 30 minutes). 100 µL of Ni-NTA beads suspension (Qiagen) pre-washed with 1 mL buffer (150 mM NaCl, 15 mM Tris, 10 mM imidazole, pH 7.5) for 3 times were then added to the lysate (supernatant) and incubated with gentle mixture at room temperature for 1 hour. The resins were then spun down at low speed (2000 ×g) for 5 minutes at 4°C. The supernatant was removed and the beads were loaded to a Micro Bio-Spin column (Bio-Rad). The Ni-NTA beads were then washed with 10 mL wash buffer (150 mM NaCl, 15 mM Tris, 10 mM imidazole, pH 7.5) and the protein was eluded with 150 µL elution buffer (150 mM NaCl, 15 mM Tris, 300 mM imidazole, pH 7.5). Protein monomers were kept at 4 °C. For the purification of PlyA and PlyB monomers which contained cysteine, all buffers mentioned above were supplemented with 0.1% 2-mercaptoethanol.

Liposome preparation

Cholesterol-sphingomyelin liposomes were used for assisting the oligomerization of two component pleurotolysin nanopores (PlyAB). 25 mg cholesterol and 25 mg sphingomyelin were dissolved in 5 mL pentane with 0.5% v/v ethanol. The lipid solvent was transferred to a round flask and dispersed around the internal wall by slow rotation and heated using a hairdryer. The round flask was kept open at room temperature for 30 minutes to let the pentane evaporate completely. Then, 5 mL SDEX buffer (150 mM NaCl, 15 mM Tris, pH 7.5) was added to resuspend the lipid and the mixture immersed into a sonication bath for 5 minutes. Liposomes were 10 mg/mL in concentration and stored at -20 °C.

Oligomerization of PlyAB nanopores

PlyAB oligomerization required the first association of PlyA monomer to the liposomes. PlyA monomers were mixed with cholesterol-sphingomyelin liposomes in a 1:10 mass ratio and kept at ambient temperature for 10 minutes. Then, PlyB monomers (same amount as PlyA) were added into the lipoprotein mixture and kept for 2 hours at room temperature (liposome: PlyA : PlyB = 10 : 1 : 1, mass

ratio). PlyAB lipoprotein were stored at 4 °C and 0.5 µL of the lipoprotein were directly added to solution in chamber for getting pores in electrophysiology measurement.

Directed evolution of PlyB

PlyB mutant libraries were constructed by two PCR steps. In the first step, ~200 ng of wild type PlyB plasmid was used as template in a 50 µL PCR reaction (2 µM T7 promoter primer, 2 µM terminator primer, 25 µL REDTaq ReadyMix). The PCR protocol started with a pre-denaturing step at 95 °C for 150 seconds, followed by 30 cycles of denaturing at 95 °C for 15 seconds, annealing at 55 °C for 15 seconds and extension at 72 °C for 180 seconds. After the PCR cycles, a final extension step at 72 °C for 300 seconds was performed. REDTaq is a polymerase with relatively low fidelity (2.28 errors per 10^5 basepairs) and 68.4% of the final molecules contain one mutation after 30 cycles amplification of a 1 kb DNA template. Since PlyB gene contains 1461 base pairs, we expect around 1–2 mutations per gene after the amplification protocol. The product (MEGA primer) obtained in the first PCR was purified with QIAquick PCR purification kit and used as primer for the second step PCR in which the whole plasmids amplified using the high-fidelity polymerase Phire hot start II (Finnzymes). The 50 µL final PCR mix contained: 1 µL Phire II, 10 µL 5 x Phire buffer, 0.2 mM dNTPs, 1 µL product from first PCR (200 ng/µL), 1 µL wild type PlyB plasmid and 33 µL PCR water. The PCR reaction was conducted with a protocol: pre-incubation at 98 °C for 30 seconds, 25 cycles of denaturing and extension (denature: 98 °C for 5 seconds, extension: 72 °C for 240 seconds). The original plasmid template was eliminated by addition of DpnI (1 FDU) after incubation at 37 °C for 1 hour. 1 µL of the treated product was transferred to 50 µL of *E. cloni*® 10G competent cells (Lucigen) by electroporation. Cells were grown overnight at 37 °C on agar plate containing 100 µg/mL ampicillin. In next day, all clones were harvest from the plate and used for plasmid preparation. The plasmid mixture was then transferred into *E. cloni*® EXPRESS BL21 (DE3) cell for for screening for activity. At least 190 single clones were picked and inoculated into individual dwells of 96-deep-well plates filled with 400 µL of 2YT media containing 100 µg/mL ampicillin. Wild type PlyB was also expressed as control. Clones were grown using a plate shaker overnight at 37 °C with gentle shaking. 50 µL of overnight cell growth for each clone (starters) were inoculated into a new plate containing 600 µL of fresh 2YT media with 100 µg/mL ampicillin. Seed plates were stored at 4 °C. The new cultures were grown at 37 °C with shaking until the optical density at 600 nm was around 0.6 (2~3 hours) and 0.5 mM final concentration of IPTG was then added to each well to induce overnight expression at 25 °C. Cell cultures were spun down in the second day with 2000 ×g for 30 minutes and stored at -80 °C overnight after discarding the supernatant. After overnight freezing, 300 µL of lysis buffer (150 mM NaCl, 15 mM Tris pH 7.5, 1 mM $MgCl_2$, 0.2 mg/ml lysozyme, one cOmplete™ Protease Inhibitor Cocktail tablet per 30 mL, 0.05 units/ml DNase and 0.1% 2-Mercaptoethanol) were added to each well and the pellet resuspended. The plates were then kept shaking for 3 hours at room temperature to allow cell lysis. Then, suspension was centrifuged down with 2000 ×g for 30 minutes. The soluble-expressed PlyB monomer protein of each clone will then remain in the supernatant. The hemolytic activity of each clone was tested using sheep blood. Sheep blood cell suspension was pre-washed with SDEX buffer (4000 ×g for 1 minute) until the supernatant was clear and diluted with SDEX buffer to an absorbance of around 0.8 at 650 nm. The washed sheep erythrocytes were then first supplemented with 0.01 mg/mL wild type PlyA monomer (final concentration) and kept at room temperature for 10 minutes. Then, 100 µL of erythrocyte mixture was transferred to transparent 96-well plates and 5 µL of lysate (supernatant) from PlyB expressed clone was added to each well. The hemolytic activity was monitored by the monitoring the decrease in optical density at 650 nm with Multiskan GO Microplate Spectrophotometer (Thermo). The most active clones

represented higher soluble expression or increased toxicity of PlyB. The clones that were more highly hemolytic active were isolated and grown on large scale for sequencing and individual mutant characterization. The desired mutants were used as the template for next round directed evolution.

Single molecule electrophysiology measurement and data analysis

The electrophysiology chamber consisted of two compartments (*cis* and *trans*) separated by a 25 µm-thick polytetrafluoroethylene film (Goodfellow Cambridge Limited) containing a ~100 µm hole at its center where a drop (~10 µL) of 5% v/v hexadecane in pentane was loaded. 500 µL of buffer was then introduce into both compartments, and 10 µL of 10 mg/ml 1,2-diphytanoyl-*sn*-glycero-3-phosphocholine (DPhPC) in pentane was loaded into each chamber to form a lipid bilayer. The potential was applied and currents red using Ag/AgCl electrodes connected the two compartments and to a patch clamp amplifier (Axopatch 200B, Axon Instruments). The signal was then digitized using a Digidata 1440 A/D converter (Axon Instruments). The ground electrode was connected to the c*is* compartment and the working electrode to *trans* side. The signal was recorded using Clampex 10.4 software (Molecular Devices) and analysed using Clampfit (Molecular Devices). The dwell time, the inter-event time, the ionic current blockade (I_B) and the open pore currents (I_o) were determined using the "single channel search" function of Clampfit. Ires% values, defined as I_B/I_o x 100%, were used to describe the blockade amplitude for each event. The average dwell and inter-event times were calculated by fitting single exponentials to histograms of cumulative distribution of individual events.

PlyAB nanopore ion selectivity measurement

The ion selectivity (Na^+/Cl^-) of PlyAB nanopore was calculated using the Goldman−Hodgkin−Katz equation[1]:

$$\frac{P_{\mathrm{Na}^+}}{P_{\mathrm{Cl}^-}} = \frac{[a_{\mathrm{Cl}^-}]_{\mathrm{trans}} - [a_{\mathrm{Cl}^-}]_{\mathrm{cis}} \exp\left(\frac{V_r \mathcal{F}}{RT}\right)}{[a_{\mathrm{Na}^+}]_{\mathrm{trans}} \exp\left(\frac{V_r \mathcal{F}}{RT}\right) - [a_{\mathrm{Na}^+}]_{\mathrm{cis}}} \tag{S1}$$

where R the gas constant, T the temperature and $\mathcal{F}$ the Faraday's constant and V_r the reversal potential measured using asymmetric salt conditions. Experiments were started by getting a single channel in symmetric salt condition (400 µL, 1 M NaCl, 15 mM Tris, pH 7.5 buffer in both compartments) and the electrodes were balanced. Then, 400 µL of 3 M NaCl was added to the *cis* chamber and the same volume of salt-free buffer was added into the *trans* chamber to create a salt gradient (*cis* : *trans*, 500 mM : 2 M). The ion activity was calculated by multiplying the molar concentration of the ion with the mean ion activity coefficients (0.681 for 500mM NaCl, and 0.668 for 2000mM NaCl[2]) The solution in both sides was mixed gently and I-V curves were collected to obtain the reversal potentials.

PlyAB homology model construction

The PlyAB nanopore structure was built with homology modelling, using the MODELLER software package,[3] from the PlyAB cryo-EM map[4] and crystal structures of soluble PlyA (PDB ID: 4OEB[4]) / PlyB (PDB ID: 4OEJ[4]) monomers. Briefly, a 'prepore' full atom structure was constructed by aligning 12 copies of the soluble PlyB monomer and 24 copies of the PlyA monomer to the C-alpha atoms of the PlyAB cryo-EM structure (using PyMOL and the 'super' alignment command). The full sequence of PlyAB, together with the positional information given by the C-alpha atoms in the cryo-EM structure and that of the pre-pore

(barring those residues involved in the transmembrane region), were then fed into the 'automodel' class of MODELLER, allowing it to construct several full-atom homology models. The best model (*i.e.* the one with the lowest DOPE score) was then fitted to the PlyAB cryo-EM map using simulated annealing molecular dynamics optimization as implemented in the Flex-EM[5] extension of MODELLER. Further refinement of the structure was carried out using symmetry constrained molecular dynamics flexible fitting (MDFF) to the Cryo-EM map with NAMD[6,7] for 5 ns, followed by 5 cycles of thermal annealing (heating from 25 K to 350 K + cooling from 350 K to 300 K in steps of 10 ps per 25 K) and a 5 ns equilibration at 300 K with light (0.1 kcal/mol/Å^2) harmonic constraints on the C-alpha atoms. The homology models of PlyAB-E (PlyA: C62S, C94S; PlyB: N26D, N107D, G218R, A328T, C441A, A464V) and PlyAB-R (PlyA: C62S, C94S; PlyB: N26D, K255E, E260R, E270R, A328T, C441A, A464V) were created from the homology model of the wild type structure using VMD[8] and their was energy minimized using a constrained molecular dynamics run (100 ps) with NAMD.

PlyAB ePNP-NS simulations

Governing equations. The transport of water and ions through a nanopore can be modelled by using the Poisson-Nernst-Planck and Navier-Stokes (PNP-NS) equations. To accurately predict the transport properties of biological nanopores, we developed a set of extended PNP-NS (ePNP-NS) equations that attempt to correct for several shortcomings of the original equations, including steric ion-ion and ion-wall interactions, and concentration dependent electrolyte properties. A full description of this methodology, equations and parameters will be published in a separate work.[9] The final set up equations are given below.

The Poisson equation relates the electrostatic potential to the charge densities in the system:

$$\nabla \cdot (\varepsilon_0 \varepsilon_r \nabla \varphi) = -\left(\rho_{\text{pore}}^f + \rho_{\text{ion}}\right), \tag{S2}$$

with ε_0 the vacuum permittivity, ε_r the local relative permittivity, φ the electrostatic potential and ρ_{pore}^f and ρ_{ion} are the charge densities due to the fixed charges of pore and the mobile ions in the electrolyte, respectively. The latter is given by

$$\rho_{\text{ion}} = \mathcal{F}\sum_i z_i c_i, \tag{S3}$$

with $\mathcal{F}$ the Faraday constant, and z_i and c_i the charge number and local concentration of ion i, respectively. The local relative permittivity in the electrolyte is not constant however, but depends on the local ion concentration

$$\varepsilon_r(\langle c \rangle) = \varepsilon_r^0 \varepsilon_r^c(\langle c \rangle), \tag{S4}$$

where $\langle c \rangle = {}^1\!/_n \sum_i^n c_i$ is the local average ion concentration, ε_r^0 the relative permittivity of pure water and $\varepsilon_r^c(\langle c \rangle)$ an empirical function parametrized with experimental data.

For a given ion i, the size-modified Nernst-Planck equation describes its flux due to concentration gradients, electric fields, water flow and steric hinderance

$$\mathbf{J}_i = -\left[\mathcal{D}_i \nabla c_i + z_i \mu_i c_i \nabla \phi - \mathbf{u}\, c_i + \mathcal{D}_i \boldsymbol{\beta}_i c_i\right], \tag{S5}$$

where

$$\boldsymbol{\beta}_i = \frac{a_i^3 / a_0^3 \sum_j a_j^3 \nabla c_j}{1 - \sum_j N_\mathrm{A} a_j^3 c_j} , \tag{S6}$$

and at steady-state

$$\frac{\partial c_i}{\partial t} = -\nabla \cdot \boldsymbol{J}_i = 0 , \tag{S7}$$

with $\mathbf{J}_i$ the total flux, $\mathcal{D}_i$ the local diffusion coefficient, c_i the local concentration, z_i the charge number, μ_i the local electrophoretic mobility, ϕ the electrostatic potential, $\mathbf{u}$ the water velocity field, a_i and a_0 the maximum cubic packing diameters of the ion and water molecules, respectively. As with the permittivity, the diffusivity and mobility depend on the local ion concentration $\langle c \rangle$, but also on the distance from the nanopore wall d:

$$\mathcal{D}_i(\langle c \rangle, d) = \mathcal{D}_i^0 \mathcal{D}_i^c(\langle c \rangle) \mathcal{D}_i^w(d), \text{ and,} \tag{S8}$$

$$\mu_i(\langle c \rangle, d) = \mu_i^0 \mu_i^c(\langle c \rangle) \mu_i^w(d) , \tag{S9}$$

where $\mathcal{D}_i^0$ and μ_i^0 are respectively the diffusivity and mobility at infinite dilution, $\mathcal{D}_i^c$ and $\mathcal{D}_i^w$ are empirical functions that express the dependency of the ionic self-diffusion coefficient on the local concentration and the distance from the nanopore wall, respectively. Likewise, the functions μ_i^c and μ_i^w represent the same dependencies for the ionic mobility.

The electro-osmotic flow is computed using the Navier-Stokes equation for incompressible fluids

$$(\boldsymbol{u} \cdot \nabla)(\varrho \boldsymbol{u}) + \nabla \cdot \sigma_{ij} = \boldsymbol{F} , \tag{S10}$$

with

$$\sigma_{ij} = p\mathrm{I} - \eta\left[\nabla \boldsymbol{u} + (\nabla \boldsymbol{u})^{\mathrm{T}}\right] , \tag{S11}$$

and the continuity equation for the fluid density

$$\boldsymbol{u} \cdot \nabla \varrho = 0 , \tag{S12}$$

and the divergence constraint for the momentum

$$\nabla \cdot (\varrho \boldsymbol{u}) - \boldsymbol{u} \cdot \nabla \varrho = 0 \tag{S13}$$

where $\boldsymbol{u}$ is the fluid velocity field, ϱ is the local fluid density, p is the pressure and η is the local dynamic viscosity. The body force $\boldsymbol{F} = eN_\mathrm{A}\rho_\mathrm{ion}\boldsymbol{E}$ represents the force exerted by the local mobile charge density (*i.e.* electrical double layer). The local viscosity is expressed as

$$\eta(\langle c \rangle, d) = \eta^0 \eta^c(\langle c \rangle) \eta^w(d) \tag{S14}$$

where η^0 is the viscosity at pure water, η^c and η^w are empirical functions that depend on the local ion concentration and distance from the nanopore wall, respectively. The local density

$$\varrho(\langle c\rangle) = \varrho^0 \varrho^c(\langle c\rangle) \tag{S15}$$

with ϱ^0 the density of pure water and ϱ^c an empirical function that describes its dependency on the local ion concentration.

All empirical functions and their parametrization can be found in a separate publication.[9]

PlyAB geometry. The 2D-axisymmetric geometry of the PlyAB pore was derived from the full atom structure by first computing its 3D atomic density map on a 0.05 nm resolution grid using a custom Python code implementing the following function:

$$\rho_{\mathrm{mol}} = 1 - \prod_i \left[1 - \exp\left(-\frac{-d_i^2}{(\sigma R_i)^2}\right)\right] \tag{S16}$$

with R_i the Van der Waals radius of atom i, d_i the distance of the atomic center from the centers of each location in the grid and $\sigma = 0.93$ a common width factor. The resulting density map was subsequently averaged radially around the longitudinal axis of the pore, and a final geometry of the pore was defined as a simplified version (*i.e.*, a significantly reduced amount of vertices) of the 25% contour line of the resulting 2D density map (Figure S8a).

PlyAB-E2 and -R charge distributions. The charge distribution maps of PlyAB-E2 and -R were also computed from their full atom models. Briefly, each atom i was assigned a partial charge $\delta_i$and a radius R_i, as defined by the CHARMM36 forcefield, using the PDB2PQR software package. Next, using custom Python code, the charge of each atom with coordinates (x_i, y_i, z_i) was added onto a 2D grid using the Gaussian function

$$\rho^f_{\mathrm{pore}}(r,z) = \sum_i \frac{e\delta_i}{\pi(\sigma R_i)^2} \exp\left(-\frac{-(r-r_i)^2 + (z-z_i)^2}{(\sigma R_i)^2}\right) \tag{S17}$$

with r and z the radial and longitudinal coordinates of the grid, respectively. $\sigma = 0.5$ is a sharpness factor and $r_i = \sqrt{x_i^2 + y_i^2}$. The resulting volumetric chargemaps were plotted in

Full simulation geometry and boundary conditions (BCs). The nanopore geometry ($\varepsilon_r = 20$), as defined by the 25% contour line of the radially averaged density map, was embedded into a lipid bilayer, represented by a dielectric slab (2.8 nm thickness, $\varepsilon_r = 2.8$), and surrounded by a spherical electrolyte reservoir ($r = 250$ nm). The electrostatic potential at the *cis* boundary is set to be grounded ($\varphi = 0$ V, 'grounded BC'), while at the *trans* boundary it is fixed to the applied bias voltage ($\varphi = V_{\mathrm{b}}$, 'potential BC'). Both reservoir boundaries have no normal stress on the fluid ($\sigma_{ij}\mathrm{n} = 0$, 'open boundary BC') and have fixed ion concentrations ($c_i = c_s$, 'concentration BC'), effectively mimicking an infinite reservoir of water and ions. The interface between the nanopore and lipid membrane is impermeable to ions ($-\mathrm{n} \cdot \boldsymbol{J}_i = 0$, 'no flux BC') and the water velocity is set to zero ($\boldsymbol{u} = 0$, 'no-slip BC').

Model validation. We validated our model by comparing the simulated current-voltage relationships of both PlyAB-E2 and PlyAB-R at 1 M NaCl with those measured experimentally (Figure S9), and found them to be in excellent agreement. The deviation at high negative bias voltages (for PlyAB-R) and positive bias voltages (for PlyAB-E2) is caused by the frequent gating of the nanopores at these potentials, which cannot

be captured by the simulation and results in an apparent lower and more noisy experimental conductance. In a second validation approach, we compared the equilibrium electrostatic potentials (*i.e.*, the potential at no applied bias voltage) obtained (1) *via* solving of the Poisson-Boltzmann (PB) equation on the full atom homology models of PlyAB with the Adaptive Poisson-Boltzmann Solver (APBS),[10] and (2) *via* solving the ePNP-NS equations on the 2D-axisymmetric model with COMSOL Multiphysics (Figure S10). To allow for a good comparison, the 3D potential map obtained from APBS was radially averaged along the longitudinal symmetry axis of the pore. The electrostatic differences between PlyAB-E2 and PlyAB-R are reproduced faithfully by the ePNP-NS simulation, notably the switch from the highly negative (PlyAB-E2) to predominantly positive potential (PlyAB-R) at the *cis* constriction. The potential inside the protein core of pore, particularly for $z < 5\ \mathrm{nm}$, is less accurate. The reason for this is that the central cavity between the A and B subunits is connected to the fluid reservoir in the 3D APBS simulation, resulting in proper ionic screening of the potential. This is not the case in the 2D-axisymmetric ePNP-NS simulations where, due to technical constraints, this cavity is modelled as a pure water ($\varepsilon_r = 78.15$). The absence of any ionic screening inside the pore hence gives rise to much higher potentials. Because the electrostatic potential within the nanopore lumen appears to be unaffected, we expect these differences to have little to no impact on the transport properties of either mutants.

Supplementary figures

Assisted directed evolution workflow

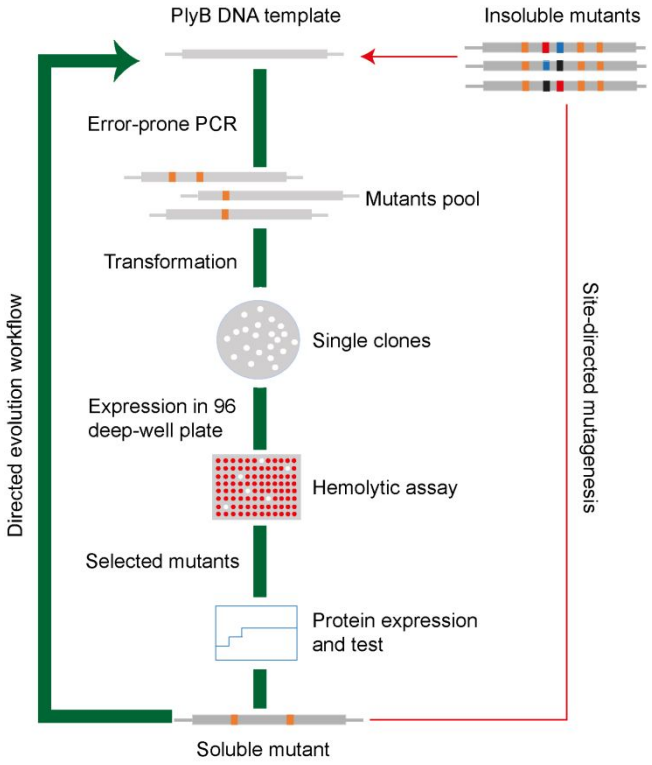

Figure S1. Workflow of the directed evolution experiments performed to engineer PlyAB nanopore. The green line shows the directed evolution workflow of nanopore engineering to increase the soluble expression of PlyB monomer. The red arrow shows the introduction of a specific mutation by site-directed mutagenesis and the further refinement of expression by directed evolution.

PlyA and PlyB oligomerization

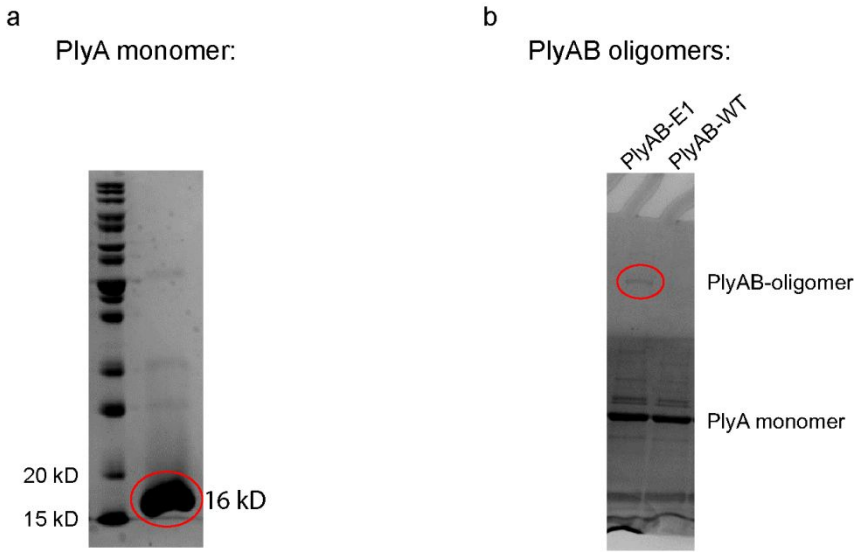

Figure S2. 12% SDS-PAGE electrophoresis of PlyA monomer and PlyAB oligomers. (a) Lane 1: Protein marker (Thermo, #26614), lane 2: PlyA monomers. (b) Lane 1: PlyAB-E1 and Lane 2: PlyAB-WT oligomers. The red circle indicated the PlyAB complex in the 4% SDS-polyacrylamide stacking gel.

Typical gating traces of PlyA-WT/PlyB-E1

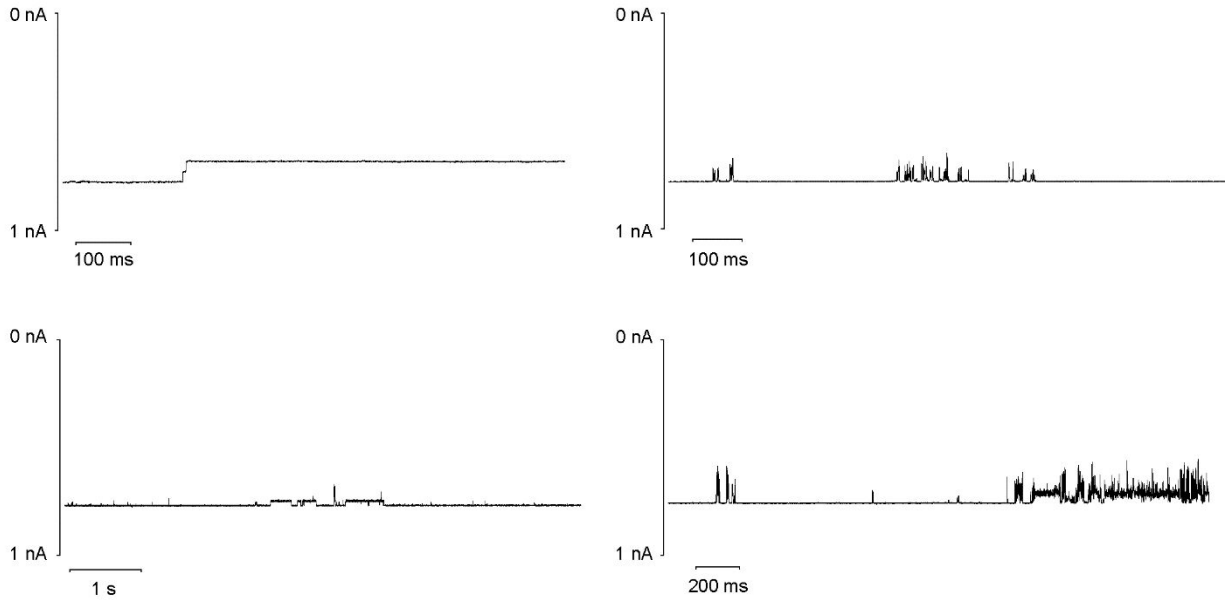

Figure S3. Typical gating traces of PlyA-WT/PlyB-E1 nanopores. Traces were recording in 1 M NaCl at pH 7.5, under -50 mV applied potential.

Improvement of pore stability after replacement of the cysteine residues in PlyA

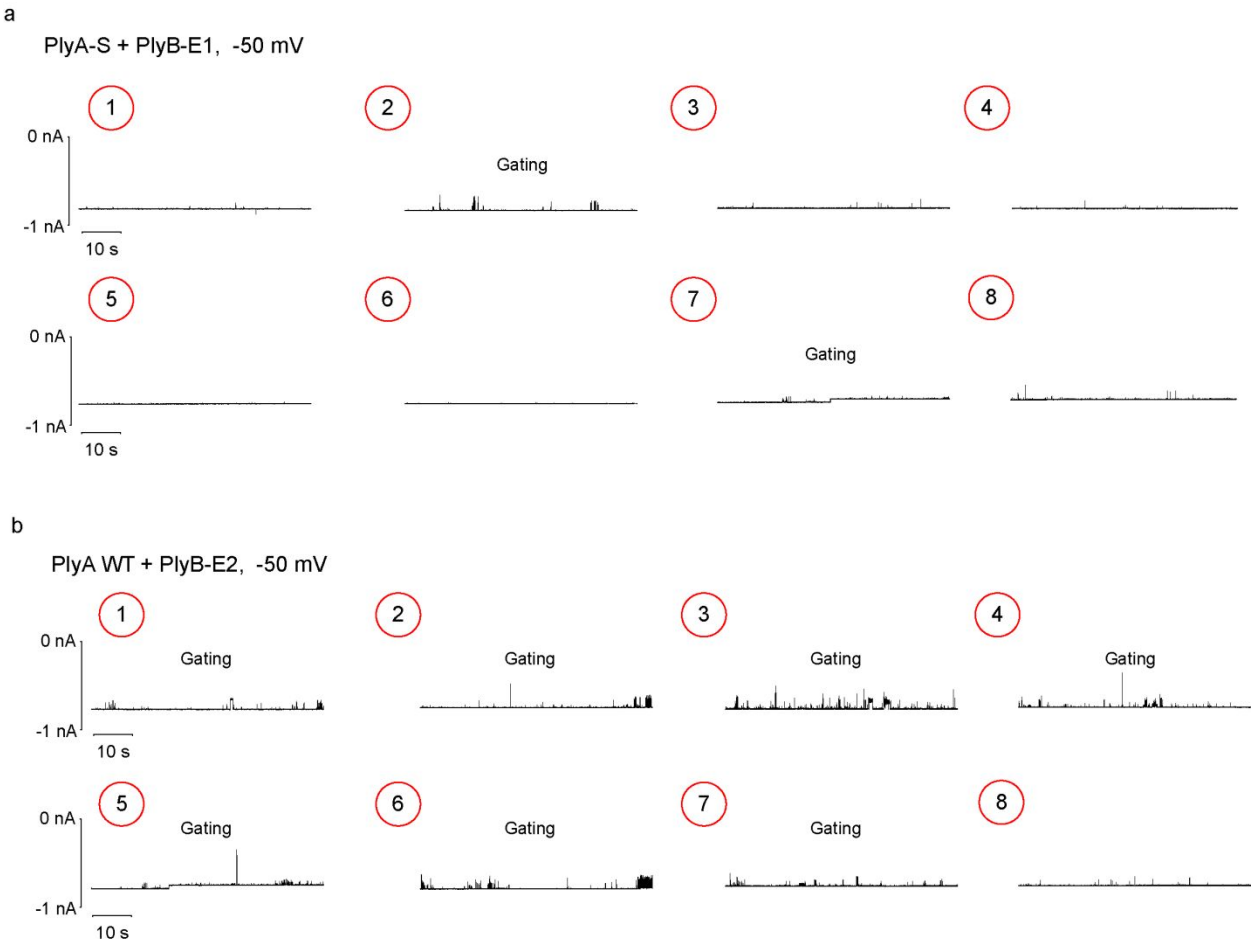

Figure S4. Improvement of pore stability after replacement of the cysteine residues in PlyA. (a) A selection of single channels of PlyAB nanopores made with cysteine-free PlyA-S and PlyB-E1. Around 20% of pores in eight showed instabilities at -50 mV (b) Eight single channels recordings obtained with WT-PlyA (which contained two cysteine residues at the lipid interface) and cysteine-free PlyB-E2 oligomers. About seventy percent of pores displayed various gating conditions under -50 mV applied potential. Channels were measured in 1 M NaCl at pH 7.5.

Electrophysiology characterization of PlyAB-E1 nanopores in 1 M NaCl

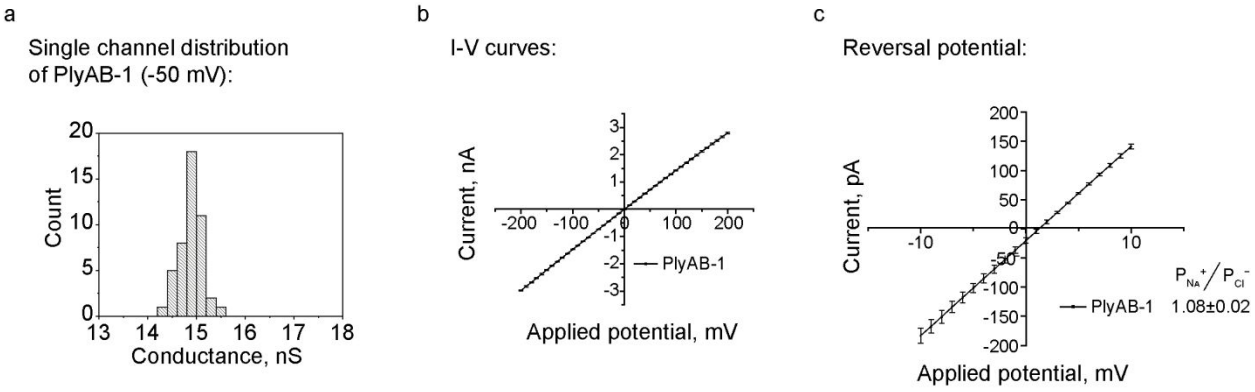

Figure S5. Electrophysiology characterization of PlyAB-E1 nanopores. (a) Single channel distribution in 1 M NaCl and pH 7.5. (b) I-V curves of PlyAB-E1 collected in 1 M NaCl and pH 7.5. (c) Reversal potential measured in asymmetric salt condition (500 mM NaCl in *trans* and 2 M NaCl in *cis*) at pH 7.5. The ion selectivity was calculated as described in methods. Error bars were standard deviations calculated with minimum 3 experiments.

Electrophysiology characterization of PlyAB-R nanopores in 300 mM NaCl and pH 7.5

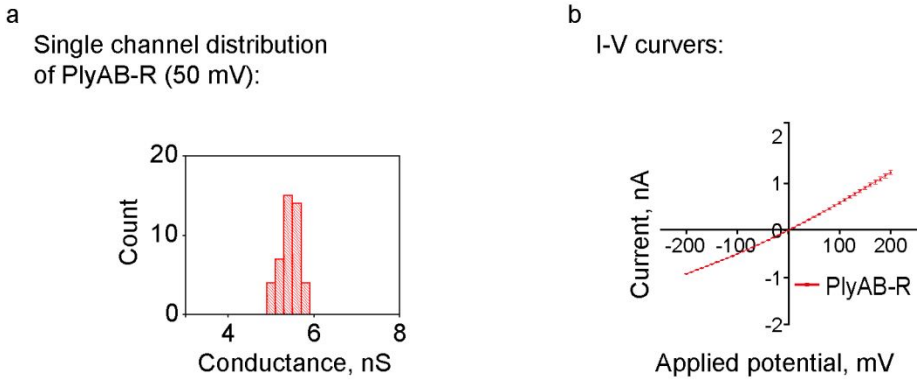

Figure S6. Electrophysiology characterization of PlyAB-R nanopores in 300 mM NaCl and pH 7.5. (a) Single channel distribution. (b) I-V curves. Error bars were standard deviations calculated with minimum 3 experiments.

Power spectrums of PlyAB-R and PlyAB-E2 nanopores

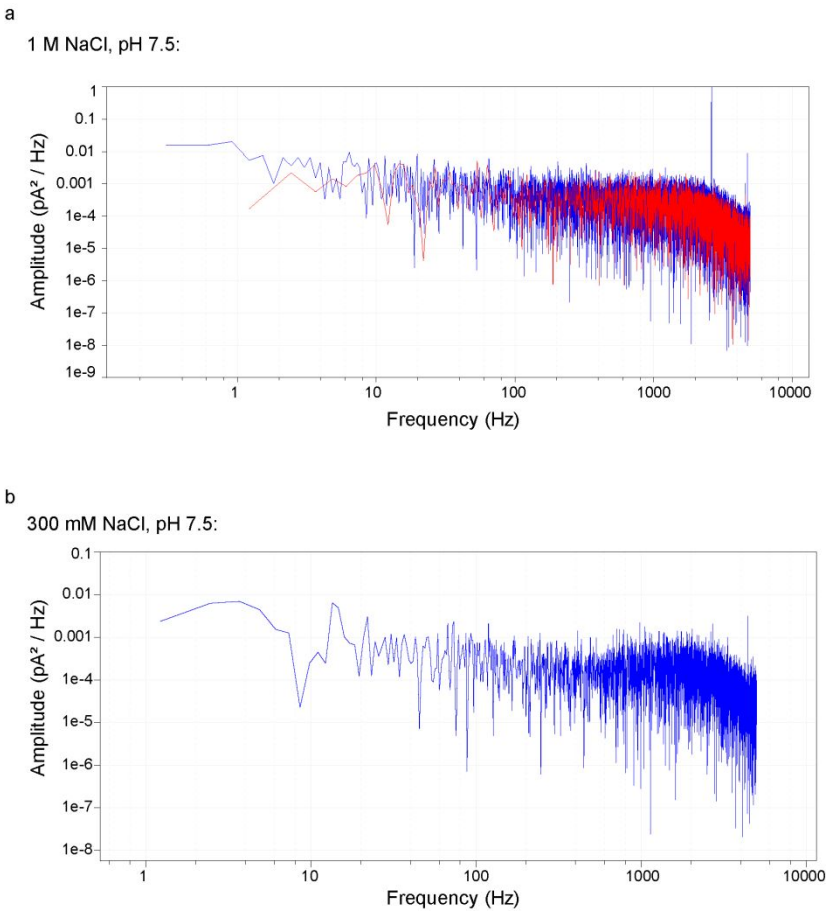

Figure S7. Power spectra of PlyAB-R and PlyAB-E2 nanopores. (a) Superimpose of PlyAB-R (blue) and PlyAB-E2 (red) determined in 1 M NaCl at pH 7.5, respectively. (b) Power spectrum of PlyAB-R determined in 300 mM NaCl and pH 7.5. The spectrums were measured under 50 mV applied potential and signal collected with a 10 kHz sampling and a 2 kHz Bessel filter.

Radial atomic density and volume charge densities of PlyAB-E2 and PlyAB-R nanopores

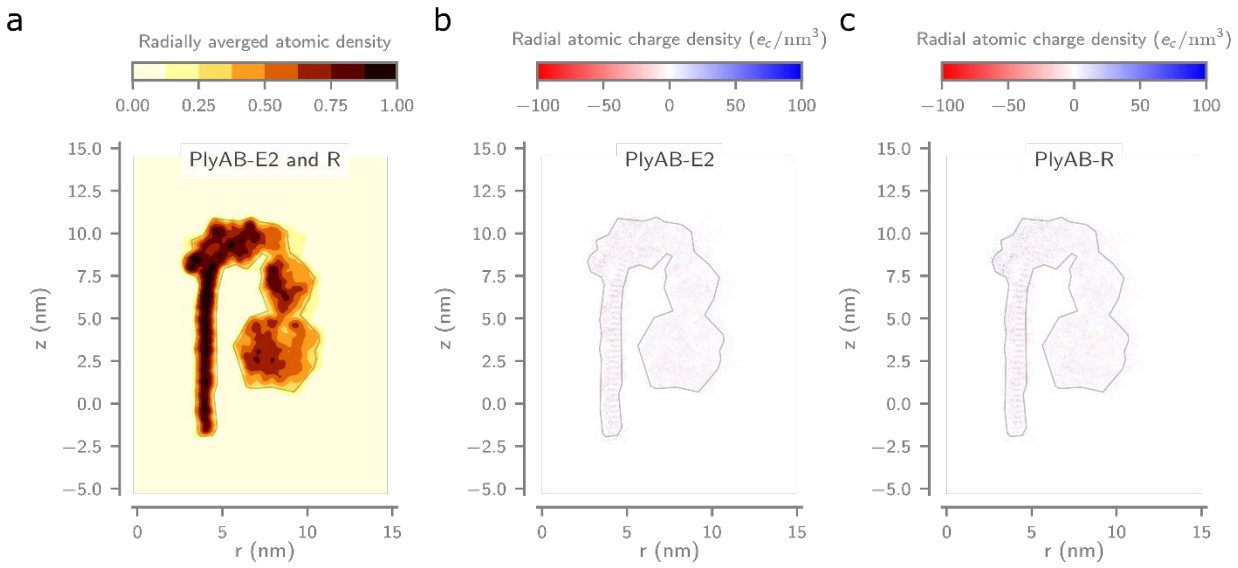

Figure S8. Radial atomic and charge densities of PlyAB-E2 and -R.(a) Contourplot of the radially averaged 3D atomic density map as computed from the full atom PlyAB homology model using Equation S16. The simplified 25% contour line used for determining the geometry of the nanopore in the continuum simulation is overlaid in grey. Radial volume charge density maps of (b) PlyAB-E2 and (c) PlyAB-R as computed using Equation S17 by summation of all atomic partial charges onto a single plane.

Comparison between the experimental and simulated (ePNP-NS) IV curves

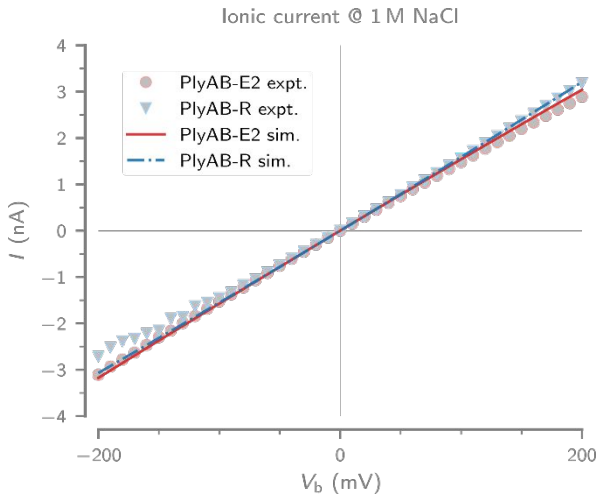

Figure S9. Comparison between the experimental and simulated (ePNP-NS) IV curves of PlyAB-E2 and -R at 1M NaCl, pH 7.5.

Comparison of the equilibrium and electrostatic profiles of PlyAB-E2 and PlyAB-R

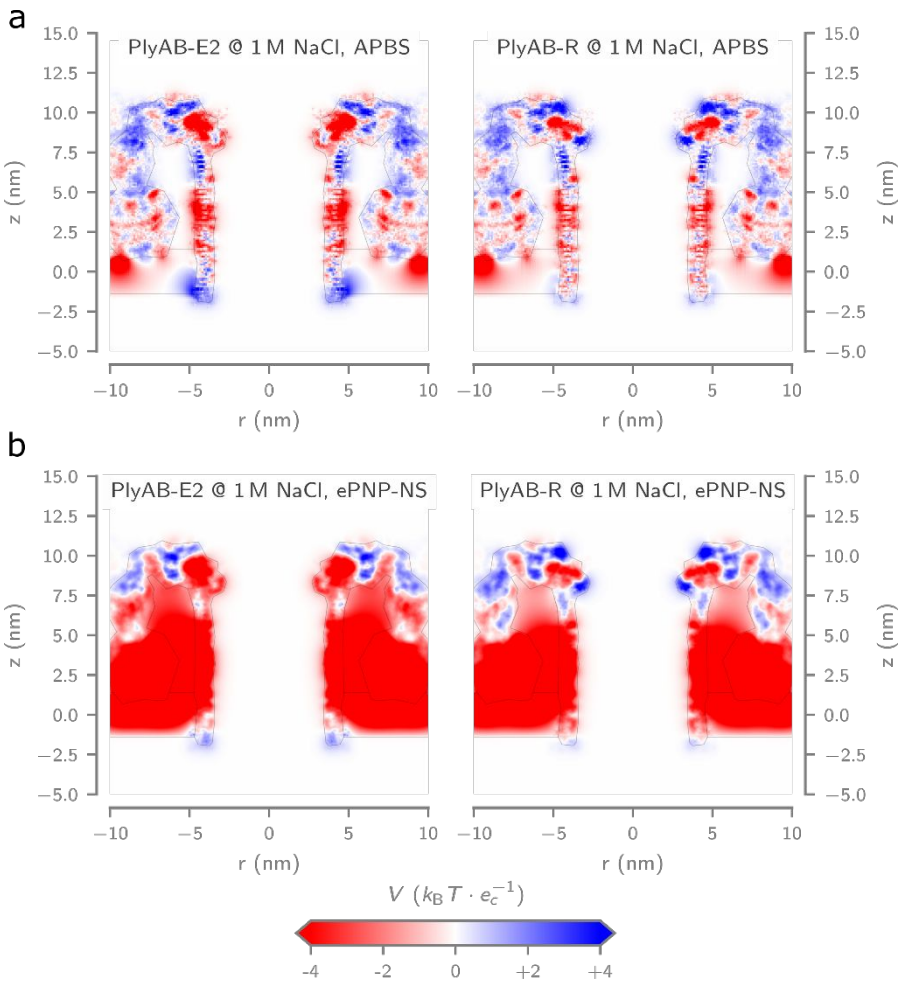

Figure S10. Comparison of the equilibrium (*i.e.*, at 0 mV transmembrane bias voltage) electrostatic profiles of PlyAB-E2 (left) and PlyAB-R (right) at 1 M NaCl as computed using (a) the Poisson-Boltzmann (PB) equation applied to the full atom homology model and, (b) the extended Poisson-Nernst-Planck Navier-Stokes (ePNP-NS) equations applied to the 2D-axisymmetric model. The PB equation was solved using the Adaptive Poisson-Boltzmann Solver (APBS), and the resulting 3D potential map was radially averaged around the longitudinal symmetry axis of the pore. The ePNP-NS equations were implemented in, and solved using, COMSOL Multiphysics 5.4. The grey outline represents the geometry used for the ePNP-NS simulations.

Simulated volumetric flow rate

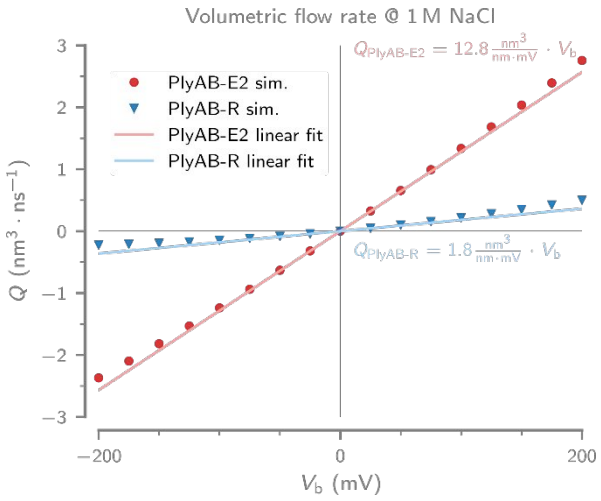

Figure S11. Simulated volumetric flow rate (Q), *i.e.* the volume of water flowing through the pore per unit of time, as a function of the applied voltage (V_b) for PlyAB-E2 and PlyAB-R in 1 M NaCl. The solid lines represent linear regression fits ($y = a \cdot x$) to the data.

Electro-osmotic flow velocity and electric field at negative bias potential

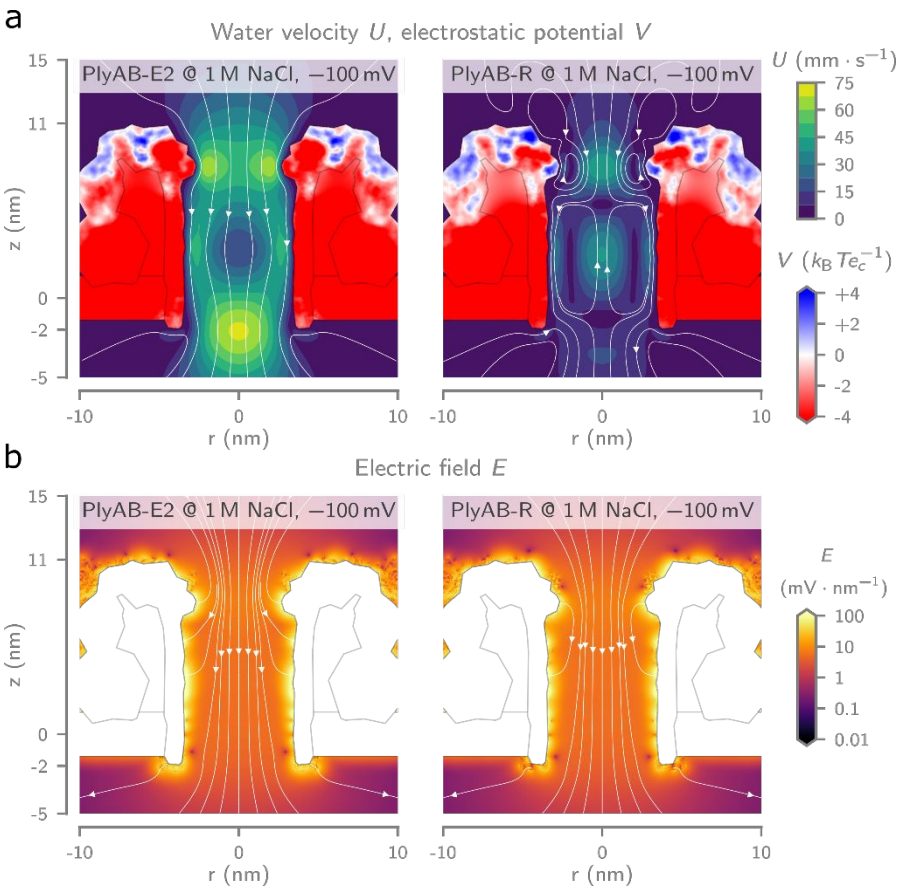

Figure S12. Electro-osmotic flow velocity and electric field at negative bias potential and 1M NaCl. (a) Electro-osmotic flow velocity contour maps of PlyAB-E2 (left) and -R (right) at −100 mV bias voltage. The white streamlines indicate the direction of the flow. The coloring inside the pore and lipid bilayer shows the local electrostatic potential profile. (b) Heatmap and streamlines of the electric field of PlyAB-E2 (left) and -R (right). Note that the electric field inside the pore is calculated in the simulation but was omitted here for clarity.

Ion concentration distribution

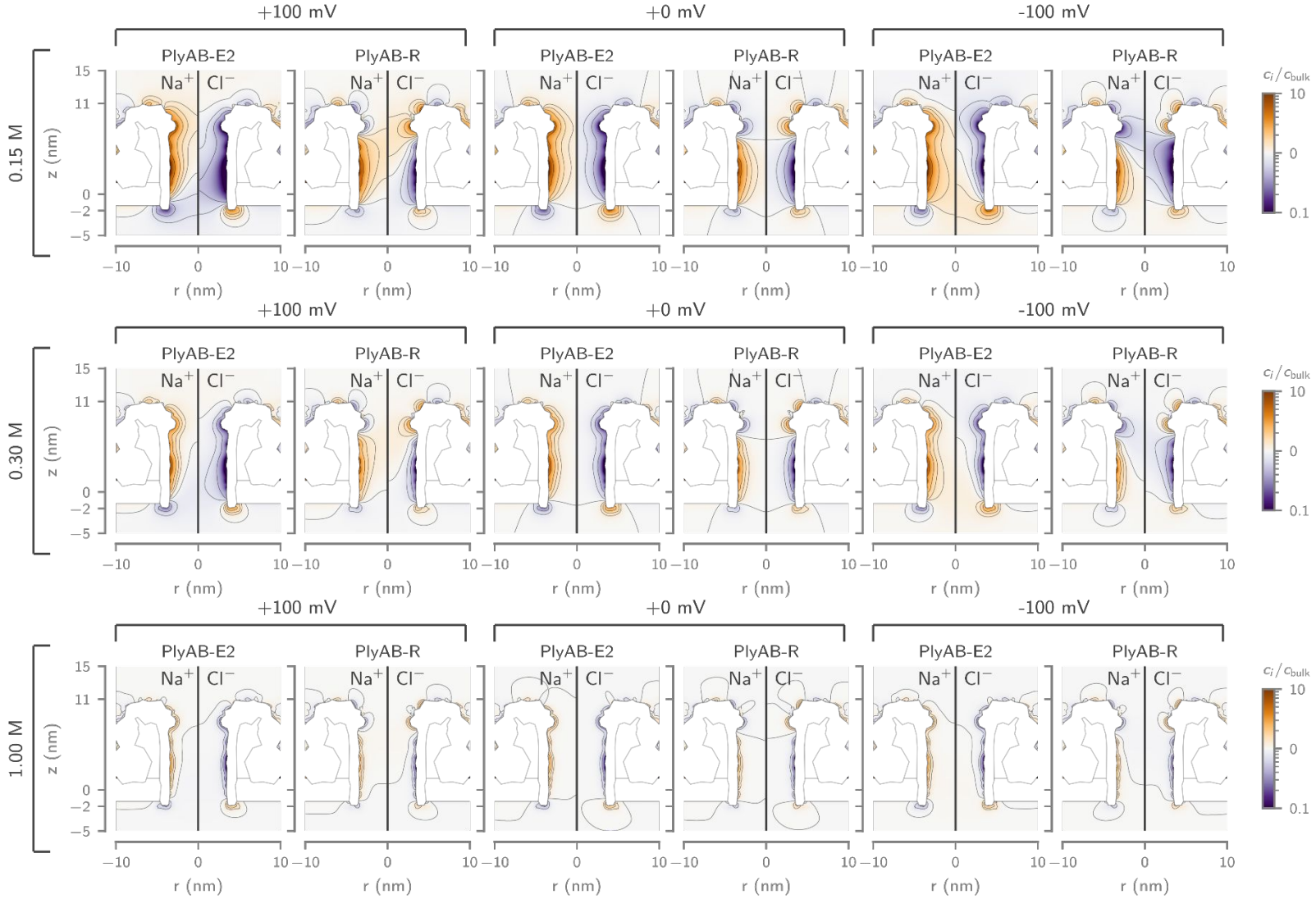

Figure S13. Ion concentration distribution in PlyAB-E2 and PlyAB-R at 0.15 M, 0.3 M and 1.0 M NaCl bulk reservoir concentrations and at +100 mV, 0 mV and -100 mV applied bias potentials.

Electric potential distribution

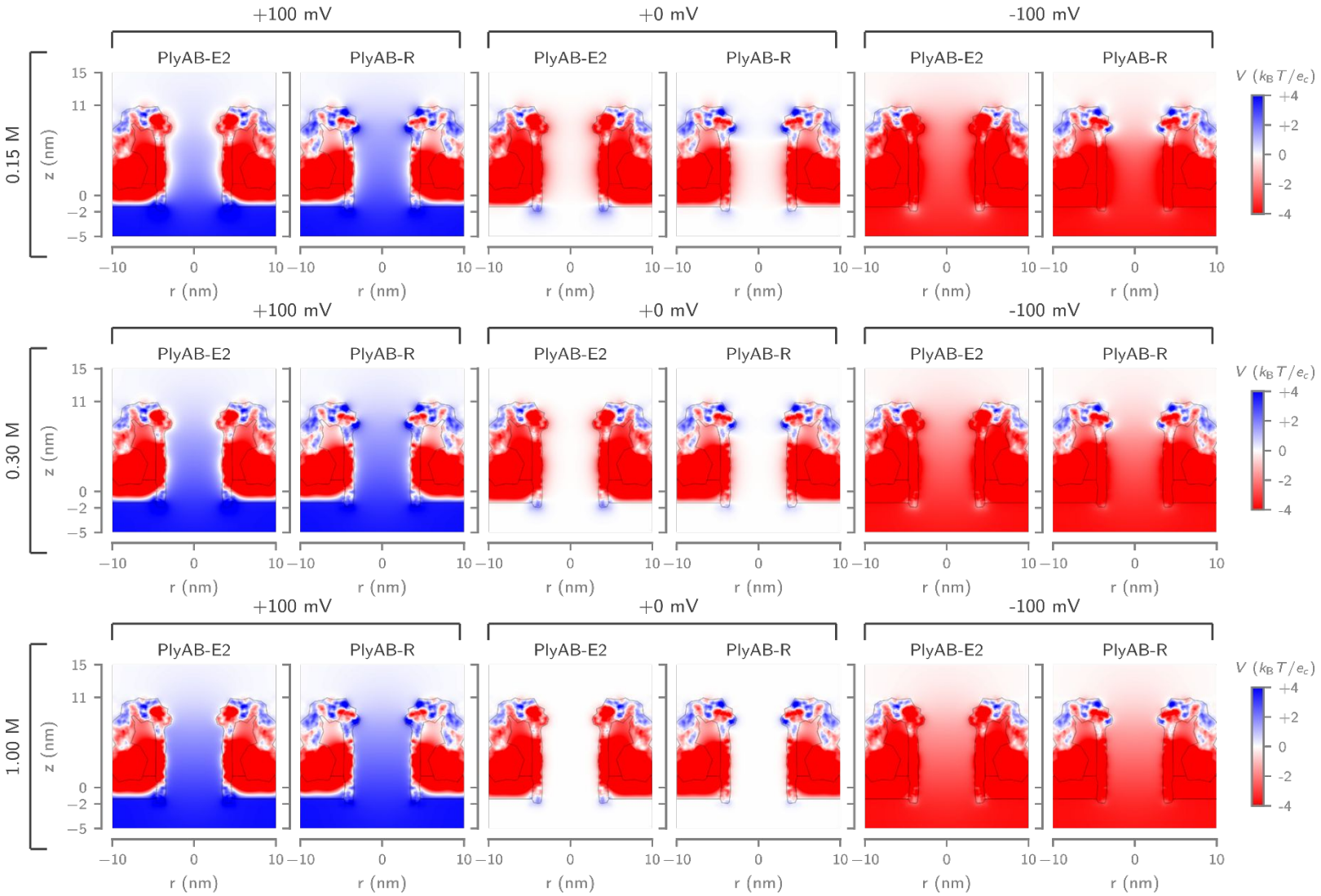

Figure S14. Electric potential distribution in PlyAB-E2 and PlyAB-R at 0.15 M, 0.3 M and 1.0 M NaCl bulk reservoir concentrations and at +100 mV, 0 mV and -100 mV applied bias potentials.

Water velocity distributions

Figure S15. Water velocity distribution in PlyAB-E2 and PlyAB-R at 0.15 M, 0.3 M and 1.0 M NaCl bulk reservoir concentrations and at +100 mV, 0 mV and -100 mV applied bias potentials.

Electric field distributions

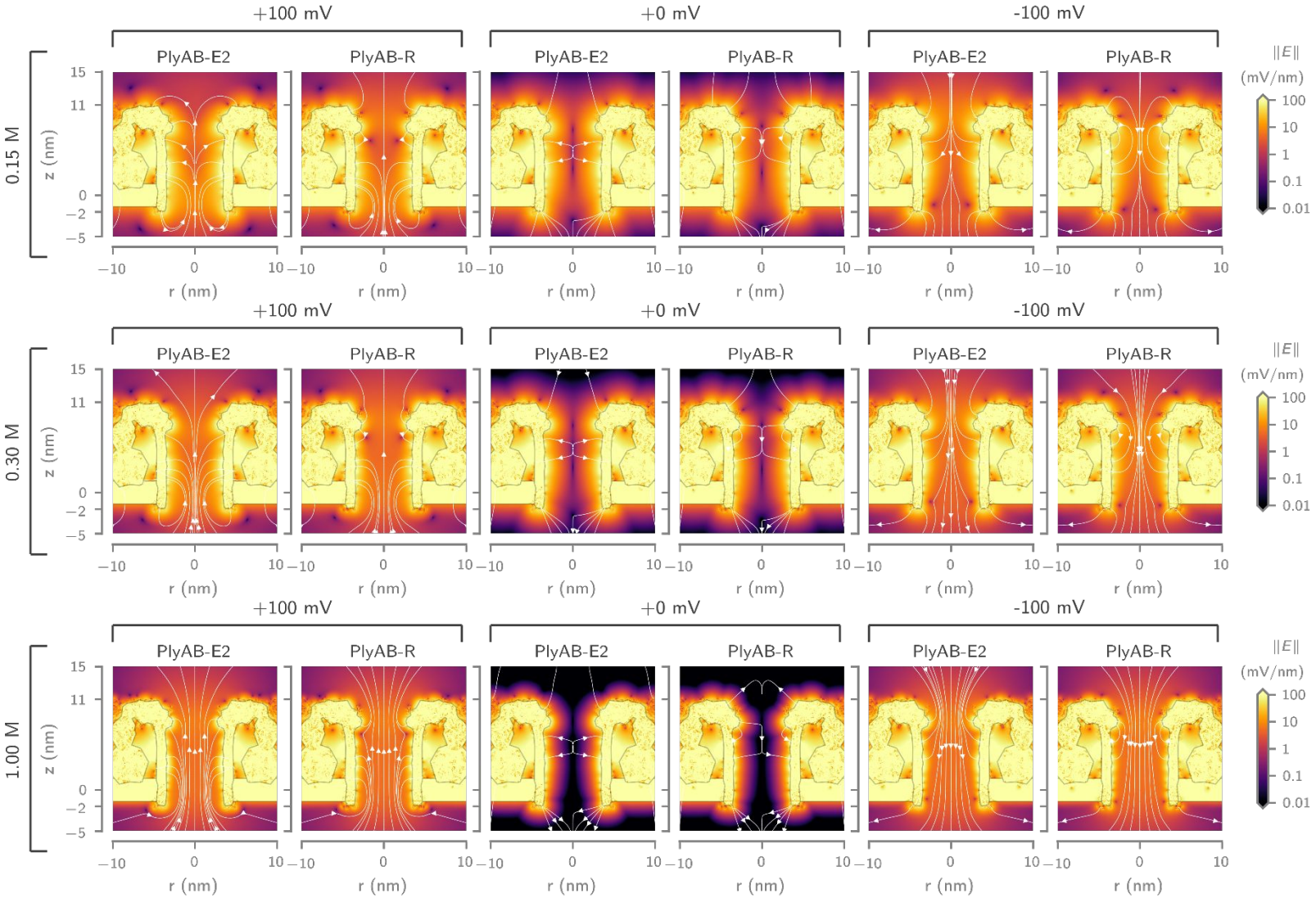

Figure S16. Electric field distribution in PlyAB-E2 and PlyAB-R at 0.15 M, 0.3 M and 1.0 M NaCl bulk reservoir concentrations and at +100 mV, 0 mV and -100 mV applied bias potentials.

Capture of BSA from the trans side of PlyAB-R under high potentials in 1 M NaCl

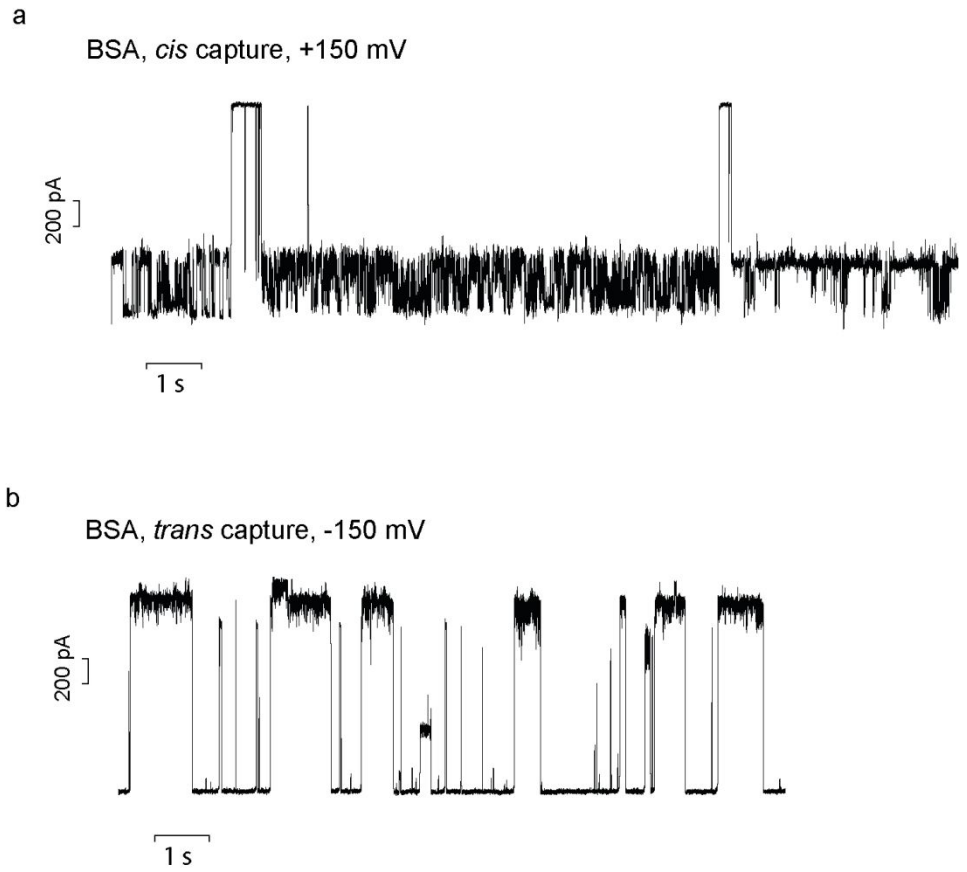

Figure S17. Capture of BSA from the *trans* side of PlyAB-R under high potentials in 1 M NaCl at pH 7.5. (a) BSA was capture from *cis* side under +150 mV potential. (b) BSA was capture from *trans* side under -150 mV potential. Recordings were collected by using a 50 kHz sampling rate and a 10 kHz low-pass Bessel filter.

Capture of human plasma proteins from the trans side of PlyAB-R in 300 mM NaCl

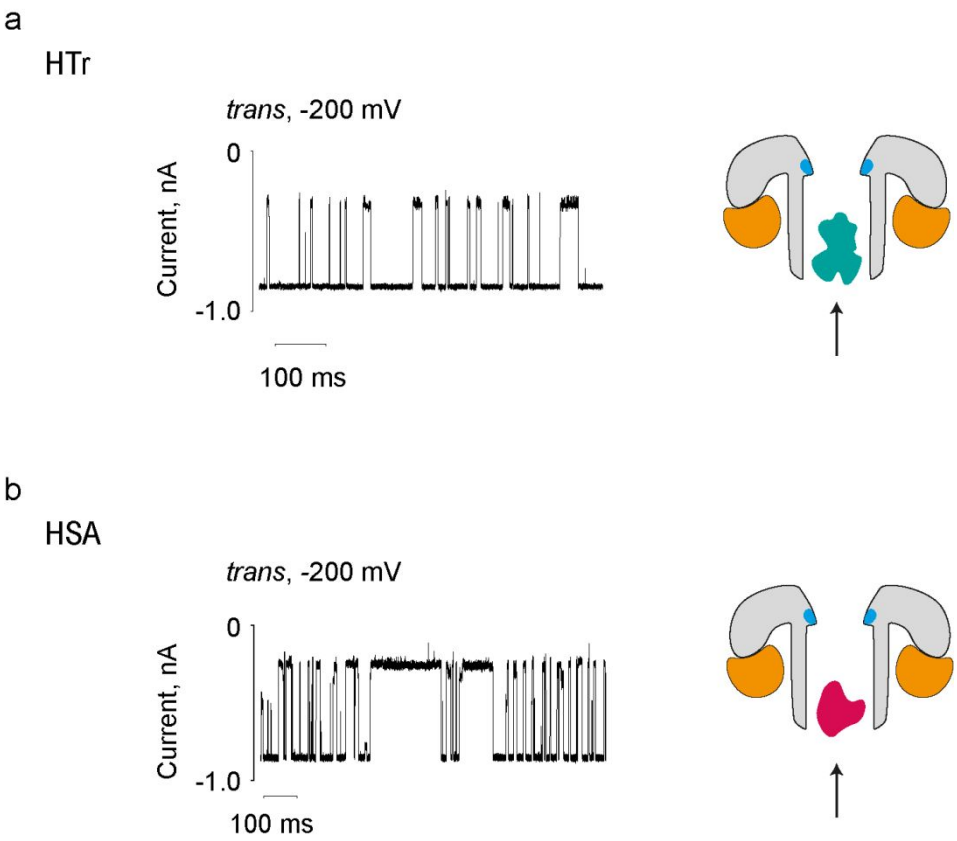

Figure S18. Capture of human plasma proteins from the *trans* side of PlyAB-R in 300 mM NaCl at pH 7.5. (a) Human transferrin (HTr) was capture from *trans* side under -200 mV potential. (b) Human serum albumin (HSA) was capture from *trans* side under -200 mV potential. Recordings were collected by using a 50 kHz sampling rate and a 10 kHz low-pass Bessel filter.

Supplementary tables

Table S1. Summary of selected PlyB mutants

Name	Mutations	Engineering path	Changes in pore lumen	Ion selectivity
PlyB-E1	N26D, A328T, A464V	3 screening rounds starting from WT-PlyB	No	Cation selective
PlyB-E2	N26D, N107D, G218R, A328T, C441A, A464V	5 screening rounds starting from WT-PlyB	N107D, G218R	Cation selective
PlyB-R	N26D, K255E, E260R, E261R, E270R, A328T, C441A, A464V	Site-directed mutagenesis on PlyB-E1, followed by 3 rounds of directed evolution. Includes cysteine replacement	K255E, E260,261,270R (to positive constriction)	Anion selective

Table S2. Conductance of PlyAB nanopores measured at pH 7.5.

Condition	Conductance, nS	S.D.	n
PlyAB-E1, 1 M NaCl, -50 mV	14.9	0.2	46
PlyAB-E2, 1 M NaCl, -50 mV	15.4	0.3	53
PlyAB-R, 1 M NaCl, +50 mV	15.3	0.8	112
PlyAB-R, 300 mM NaCl, +50 mV	5.4	0.2	44

S.D. represented the standard deviations.

Table S3. Values of the I-V curves measured with PlyAB nanopores in different salt conditions at pH 7.5.

Potential, mV	PlyAB-E1 in 1M NaCl		PlyAB-E2 in 1M NaCl		PlyAB-R in 1M NaCl		PlyAB-R in 300mM NaCl	
	pA	S.D.	pA	S.D.	pA	S.D.	pA	S.D.
-200.0	-2982.2	18.2	-3113.3	35.4	-2716.6	312.5	-922.3	5.3
-190.0	-2826.3	22.9	-2932.5	48.2	-2520.8	317.7	-882.9	1.9
-180.0	-2675.6	24.1	-2779.9	43.3	-2387.0	209.7	-840.5	4.1
-170.0	-2525.1	22.3	-2633.5	33.4	-2329.4	180.4	-802.6	2.7
-160.0	-2374.1	21.8	-2466.9	38.1	-2216.3	131.6	-758.9	4.8
-150.0	-2224.7	16.2	-2300.2	46.8	-2155.4	110.2	-717.3	4.9
-140.0	-2071.9	17.8	-2156.5	30.9	-1901.4	123.6	-674.3	0.1
-130.0	-1921.4	18.0	-1994.7	32.9	-1862.8	44.6	-634.3	1.1
-120.0	-1771.5	15.9	-1841.7	27.6	-1626.8	244.0	-590.1	1.1
-110.0	-1622.3	14.7	-1686.5	26.5	-1551.1	123.3	-545.9	0.4
-100.0	-1472.4	14.7	-1529.4	25.7	-1457.7	62.8	-500.0	0.4
-90.0	-1325.6	7.9	-1374.5	25.1	-1331.8	19.9	-454.0	0.1
-80.0	-1176.7	8.3	-1225.9	18.7	-1174.7	44.9	-406.9	0.6
-70.0	-1028.5	6.1	-1069.3	15.7	-1049.9	24.9	-358.7	0.5
-60.0	-882.3	3.9	-915.5	14.2	-899.0	17.8	-309.4	0.6
-50.0	-733.0	5.1	-760.8	12.4	-752.4	16.9	-259.3	1.0
-40.0	-587.2	3.5	-608.6	10.1	-603.9	13.0	-208.6	1.6
-30.0	-439.5	4.4	-456.6	7.5	-453.7	9.7	-156.8	2.2
-20.0	-292.8	5.4	-304.6	5.7	-303.4	6.4	-104.3	2.9
-10.0	-147.2	5.7	-153.2	4.5	-152.1	3.9	-51.0	3.5
0.0	-1.8	6.5	-1.8	4.7	0.1	3.9	3.4	4.7
10.0	143.4	7.5	148.9	5.7	152.9	6.1	58.4	5.7
20.0	287.6	8.5	298.8	7.2	306.6	9.0	114.3	6.8
30.0	431.7	9.7	448.9	10.2	460.7	11.6	170.9	8.6
40.0	575.0	10.7	597.6	11.2	615.7	14.3	228.0	9.9
50.0	717.6	12.7	744.4	13	771.5	16.2	286.4	11.2
60.0	861.7	13.3	892.7	16.2	927.7	18.6	345.0	13.1
70.0	1003.3	14.6	1040.2	17.9	1084.8	20.9	404.4	15.4
80.0	1143.5	15.6	1187.3	19.1	1242.5	23.6	464.5	17.6
90.0	1283.6	18.6	1332.7	20.4	1401.3	25.1	525.5	18.9
100.0	1425.5	18.2	1477.4	22.3	1559.3	28.5	584.8	24.2
110.0	1564.6	19.4	1624.9	26.1	1718.2	30.3	647.7	22.1
120.0	1704.6	21.6	1768.3	29.1	1878.1	32.7	712.2	25.1
130.0	1842.2	23.0	1909.5	33	2039.2	34.9	774.3	30.5
140.0	1982.6	23.6	2044.9	37.1	2200.4	36.3	835.3	33.7
150.0	2120.7	25.8	2189.2	37.6	2362.4	36.3	901.4	34.3
160.0	2254.4	23.0	2332.3	41.4	2526.0	38.1	967.1	36.6
170.0	2392.8	27.4	2471.9	50.7	2687.2	42.5	1030.0	42.0
180.0	2526.0	29.1	2608.7	47.7	2851.5	45.6	1092.1	49.0
190.0	2661.9	26.5	2748.8	50.2	3015.2	45.8	1159.7	49.4
200.0	2793.0	29.2	2886.1	50.1	3183.7	44.1	1231.8	45.8

S.D. represented the standard deviations calculated from minimum three repeats.

Table S4. Reversal potential of PlyAB nanopores measured in 1 M NaCl at pH 7.5 and the calculated ion selectivity.

Condition	Reversal potential, mV	Ion selectivity
PlyAB-E1	1.24±0.2	1.08±0.02
PlyAB-E2	1.10±0.28	1.07±0.02
PlyAB-R	-0.90±0.57	0.94±0.04

Table S5. Values of the I-V curves collected under asymmetric salt conditions with PlyAB nanopores for reversal potential and ion selectivity determination. Measurements were conducted at pH 7.5 and details of the experiment and calculation were described in Methods part.

Potential, mV	PlyAB-E1		PlyAB-E2		PlyAB-R	
	pA	S.D.	pA	S.D.	pA	S.D.
-30.0	-515.4	29.9	-491.0	17.2	-466.2	38.3
-29.0	-498.5	28.4	-474.9	17.0	-449.9	37.7
-28.0	-482.1	27.5	-459.1	16.3	-434.5	36.6
-27.0	-465.1	26.7	-442.8	16.1	-418.2	35.4
-26.0	-447.6	24.9	-426.6	15.8	-402.1	34.3
-25.0	-431.4	24.3	-410.7	14.8	-386.2	33.5
-24.0	-414.5	23.6	-394.9	14.6	-370.2	32.4
-23.0	-397.7	23.8	-378.9	14.3	-354.2	31.5
-22.0	-381.7	22.9	-362.7	13.2	-338.1	30.7
-21.0	-364.9	22.3	-346.9	13.5	-322.2	29.5
-20.0	-348.0	20.9	-331.3	12.9	-305.8	28.0
-19.0	-331.6	19.3	-315.4	12.6	-290.1	27.1
-18.0	-315.1	18.9	-299.5	12.1	-273.9	26.1
-17.0	-298.5	18.0	-283.6	11.9	-258.0	25.2
-16.0	-282.1	17.6	-268.0	11.2	-242.0	24.0
-15.0	-264.7	15.4	-252.1	11.1	-226.1	23.1
-14.0	-248.6	15.5	-236.2	10.9	-209.9	22.0
-13.0	-231.8	13.6	-220.4	10.5	-194.0	21.0
-12.0	-215.4	12.5	-204.7	10.1	-178.0	19.9
-11.0	-199.5	12.7	-189.0	9.3	-161.9	18.8
-10.0	-183.0	12.9	-173.2	9.1	-146.0	17.8
-9.0	-167.2	11.7	-157.6	8.6	-129.6	16.6
-8.0	-150.7	10.9	-141.9	8.1	-113.7	15.7
-7.0	-133.9	9.9	-126.2	7.7	-98.0	14.8
-6.0	-117.7	9.6	-110.5	7.5	-82.0	13.9
-5.0	-101.5	8.2	-95.0	6.9	-65.8	12.7
-4.0	-85.2	7.7	-79.1	5.7	-50.0	11.7
-3.0	-69.1	6.9	-63.8	6.0	-34.0	10.8
-2.0	-52.8	6.2	-48.3	5.7	-18.0	9.9
-1.0	-36.7	5.3	-32.7	5.2	-2.2	8.9
0.0	-20.3	4.6	-17.1	4.9	14.1	7.8
1.0	-4.1	3.6	-1.5	4.3	30.1	6.9
2.0	12.0	2.9	13.8	4.0	45.9	5.9
3.0	28.2	2.1	29.3	3.6	61.9	4.9
4.0	44.5	1.5	44.8	3.3	78.0	4.1
5.0	60.7	1.4	60.3	2.8	93.8	3.2
6.0	76.8	1.7	75.6	2.4	109.9	2.5
7.0	92.9	2.3	91.0	1.9	125.8	2.2
8.0	109.0	3.0	106.4	1.7	141.8	2.0
9.0	125.2	3.8	121.8	1.3	157.9	2.5
10.0	141.1	4.5	137.3	1.0	173.9	3.1
11.0	157.2	5.5	152.4	0.7	189.7	4.0
12.0	173.0	5.9	168.0	0.7	205.7	4.8
13.0	188.5	5.7	183.1	0.9	221.9	5.7
14.0	205.2	7.8	198.3	1.4	237.5	6.5
15.0	221.4	8.9	213.6	1.6	253.7	7.6
16.0	235.6	7.2	228.9	1.9	269.7	8.4
17.0	252.9	9.9	243.8	2.4	285.4	9.4
18.0	269.2	11.4	259.3	2.5	301.5	10.3
19.0	283.2	9.3	274.4	3.1	317.4	11.3
20.0	300.6	12.5	289.5	3.3	333.0	12.0
21.0	316.8	14.0	304.9	3.6	349.2	13.2
22.0	332.8	14.7	320.1	4.0	365.2	14.2
23.0	347.7	14.5	335.7	5.0	381.7	15.6
24.0	364.6	16.8	349.4	3.4	397.9	16.5
25.0	380.2	17.5	365.0	5.4	413.3	17.3
26.0	396.3	18.4	380.0	5.8	429.3	18.4
27.0	412.1	19.2	395.1	6.6	445.4	19.2
28.0	428.3	20.2	410.0	6.8	461.4	20.2
29.0	443.6	21.2	425.1	7.0	477.4	21.3
30.0	455.8	15.3	440.4	7.4	493.9	22.3

S.D. represented the standard deviations calculated from minimum three repeats

Table S6. Parameters for protein measurements with PlyAB nanopores in 1 M NaCl, pH 7.5.

Condition	Ires%	Dwell time, ms	Capture frequency, $S^{-1}\mu M^{-1}$
β-casein, *trans,* PlyAB-E1, +50 mV	84.9±1.6	8.1±1.3	166.5±3.4
β-casein, *trans*, PlyAB-E2, +50 mV	84.2±0.1	25.0±6.3	174.5±120.9
β-casein, *trans,* PlyAB-R, -50 mV	93.8±0.5	1.6±0.1	50.6±2.6
β-casein, *cis*, PlyAB-R, +50 mV	93.9±1.1	2.8±1.7	135.1±95.9
BSA, *trans,* PlyAB-R, -120 mV	40.9±1.4%	22.0±13.6	365.6±58.9
BSA, *cis*, PlyAB-R, +120 mV	38.4±0.1%	177.1±138.6	527.7±296.1

Table S7. Parameters for human transferrin (HTr) measurements with PlyAB-R nanopores in 300 M NaCl, pH 7.5.

Condition		Ires%	Dwell time, ms	Capture frequency, $S^{-1}\mu M^{-1}$
From *cis*	+50 mV	33.5±1.1	30.3±5.4	11.1±6.4
From *trans*	-200 mV	37.7±0.1	5.4±0.8	157.3±136.6

Table S8. Parameters for human serum albumin (HSA) measurements with PlyAB-R nanopores in 300 M NaCl, pH 7.5.

Condition		Ires%	Dwell time, ms	Capture frequency, $S^{-1}\mu M^{-1}$
From *cis*	+50 mV	46.3±0.9	118.5±43.0	54.2±25.8
From *trans*	-200 mV	41.3±0.1	4.1±0.7	5853.5±1619.5

References

(1) Gu, L. Q.; Serra, M. D.; Bryan Vincent, J.; Vigh, G.; Cheley, S.; Braha, O.; Bayley, H. Reversal of Charge Selectivity in Transmembrane Protein Pores by Using Noncovalent Molecular Adapters. *Proc. Natl. Acad. Sci. U. S. A.* **2000**, *97* (8), 3959–3964.

(2) Lide, D. R. CRC Handbook of Chemistry and Physics, 84th Edition, 2003-2004. *Handb. Chem. Phys.* **2003**, *53*, 2616.

(3) Šali, A.; Blundell, T. L. Comparative Protein Modelling by Satisfaction of Spatial Restraints. J.Mol.Biol 1993, pp 779–815.

(4) Lukoyanova, N.; Kondos, S. C.; Farabella, I.; Law, R. H. P.; Reboul, C. F.; Caradoc-Davies, T. T.; Spicer, B. A.; Kleifeld, O.; Traore, D. A. K.; Ekkel, S. M.; et al. Conformational Changes during Pore Formation by the Perforin-Related Protein Pleurotolysin. *PLoS Biol.* **2015**, *13* (2), 1–15. https://doi.org/10.1371/journal.pbio.1002049.

(5) Topf, M.; Lasker, K.; Webb, B.; Wolfson, H.; Chiu, W.; Sali, A. Protein Structure Fitting and Refinement Guided by Cryo-EM Density. *Structure* **2008**, *16* (2), 295–307.

(6) Phillips, J. C.; Braun, R.; Wang, W.; Gumbart, J.; Tajkhorshid, E.; Villa, E.; Chipot, C.; Skeel, R. D.; Kalé, L.; Schulten, K. Scalable Molecular Dynamics with NAMD. *J. Comput. Chem.* **2005**, *26* (16), 1781–1802. https://doi.org/10.1002/jcc.20289.

(7) Mcgreevy, R.; Singharoy, A.; Li, Q.; Zhang, J.; Xu, D.; Perozo, E.; Schulten, K. XMDFF: Molecular Dynamics Flexible Fitting of Low-Resolution X-Ray Structures. *Acta Crystallogr. Sect. D Biol. Crystallogr.* **2014**, *70* (9), 2344–2355.

(8) Humphrey, W.; Dalke, A.; Schulten, K. Sartorius Products. *J. Mol. Graph.* **1996**, *14*, 33–38.

(9) Willems, K.; Ruić, D.; Lucas, F.; Barman, U.; Hofkens, J.; Maglia, G.; Van Dorpe, P. Modeling of Ion and Water Transport in the Biological Nanopore ClyA. *bioRxiv* **2020**, 2020.01.08.897819. https://doi.org/10.1101/2020.01.08.897819.

(10) Baker, N. A.; Sept, D.; Joseph, S.; Holst, M. J.; McCammon, J. A. Electrostatics of Nanosystems: Application to Microtubules and the Ribosome. *Proc. Natl. Acad. Sci.* **2001**, *98* (18), 10037–10041. https://doi.org/10.1073/pnas.181342398.